can be seen in Fig. 3, $\mu\beta_0$ increased with increasing λ_{max} and reached a maximum value and possibly decreased as λ_{max} became sufficiently long (*18*).

Brooker has synthesized molecules with ground states that are neutral and aromatic, zwitterionic and aromatic, as well as molecules that have weak quinonal contributions to the ground state (*10*). He has shown that one can effectively tune from bond-alternate neutral structures through polar non–bond-alternate structures to extremely polar bond-alternate structures by making appropriate choices of the aromatic-quinonal character of the end groups. Introduction of too much quinonal character in the neutral form of the molecule may not be desirable, since it could result in a very polar, aromatic ground state. Molecules like these generally have negative β since the excited-state dipole moment is usually less than the ground-state dipole moment (*11, 16*). Thus, it is important to realize that the key to successful implementation of our strategy is to have the correct energetic balance between the neutral and CT states and not to simply stabilize the CT state.

The theoretical and experimental results reported here suggest that by the correct choice of the degree of aromatic-quinonal character in the ground-state wave function it should be possible to strike the optimal compromise for relative energetics of the neutral and CT resonance forms, in effect tuning the $(\alpha_A - \alpha_D)/|t|$ to optimize β. Brooker has found that, for cyanine-like molecules, increased electronic asymmetry leads to decreased μ_{ge}^2 and λ_{max}, in qualitative agreement with the results of Fig. 1. We suggest that these observations form the basis of a procedure to maximize β for a given conjugation length.

REFERENCES AND NOTES

1. D. J. Williams, *Angew. Chem. Int. Ed. Engl.* **23**, 690 (1984).
2. _____, Ed., *Nonlinear Optical Properties of Organic and Polymeric Materials*, no. 233 of the *ACS Symposium Series* (American Chemical Society, Washington, DC, 1983).
3. S. R. Marder, J. E. Sohn, G. D. Stucky, Eds., *Materials for Nonlinear Optics: Chemical Perspectives*, no. 455 of the *ACS Symposium Series* (American Chemical Society, Washington, DC, 1991).
4. D. S. Chemla and J. Zyss, Eds., *Nonlinear Optical Properties of Organic Molecules and Crystals* (Academic Press, Orlando, FL, 1987), vols. 1 and 2.
5. C. J. Ballhausen and H. B. Gray, *Molecular Orbital Theory* (Benjamin, New York, 1964).
6. J. F. Ward, *Rev. Mod. Phys.* **37**, 1 (1965); B. J. Orr and J. F. Ward, *Mol. Phys.* **20**, 513 (1971).
7. J. L. Oudar and D. S. Chemla, *J. Chem. Phys.* 66, 2664 (1977); B. F. Levine and C. G. Bethea, *ibid.*, p. 1070; S. J. Lalama and A. F. Garito, *Phys. Rev. A* **20**, 1179 (1979).
8. J. L. Oudar and H. Le Person, *Opt. Commun.* **15**, 258 (1975); B. F. Levine and C. G. Bethea, *Appl. Phys. Lett.* **24**, 445 (1974); K. D. Singer and A. F. Garito, *J. Chem. Phys.* **75**, 3572 (1981).
9. M. M. Choy, S. Ciraci, R. L. Byer, *IEEE J. Quantum Electron.* **QE-11**, 40 (1975); D. J. Williams, *Adv. Chem. Ser.* **218**, 298 (1988); D. N. Beratan, in (*3*), pp. 89–102.
10. L. G. S. Brooker and R. H. Sprague, *J. Am. Chem. Soc.* **63**, 3203 (1941); L. G. S. Brooker *et al.*, *ibid.*, p. 3192; _____, G. H. Keyes, W. W. Williams, *ibid.* **64**, 199 (1942); L. G. S. Brooker and R. H. Sprague, *ibid.* **67**, 1869 (1945); L. G. S. Brooker, *Rev. Mod. Phys.* **14**, 275 (1942).
11. Quinonal structures have been studied previously and exhibit large negative values for β: A. F. Garito, K. D. Singer, C. C. Teng, in (*2*), pp. 1–26.; S. J. Lalama *et al.*, *Appl. Phys. Lett.* **39**, 940 (1981).
12. J. L. Bredas, *Synth. Met.* **17**, 115 (1987); _____ *et al.*, *ibid.* **28**, 533 (1989).
13. L.-T. Cheng *et al.*, *Proc. SPIE* **1147**, 61 (1989). The uncertainty in the reported β values is ±10% of the measured value.
14. K. D. Singer, J. E. Sohn, S. J. Lalama, *Appl. Phys. Lett.* **49**, 248 (1986).
15. L. G. S. Brooker and R. H. Sprague, *J. Am. Chem. Soc.* **63**, 3214 (1941).
16. The hyperpolarizability of a merocyanine dye measured in two solvents has been reported previously: B. F. Levine *et al.*, *J. Chem. Phys.* **68**, 5042 (1978).
17. M. J. Kamlet *et al.*, *J. Org. Chem.* **48**, 2877 (1983); M. J. Kamlet, J. L. M. Abboud, R. W. Taft, *Prog. Phys. Org. Chem.* **13**, 485 (1981), and references therein.
18. Since DIA is known to absorb at very long wavelengths in water, leading to nearly equal contributions from the neutral and CT resonance forms (*15*), the β value of DIA in water is expected to be much less than that in chloroform. Unfortunately, water cannot support the large dc fields used to orient the chromophores in the EFISH experiment, so it was not possible to perform measurements in this solvent.
19. A more complete discussion of error analysis is presented in L.-T. Cheng *et al.*, unpublished results.

20. The work in this paper was performed in part by the Center for Space Microelectronics Technology, Jet Propulsion Laboratory (JPL), California Institute of Technology, and was sponsored by the Strategic Defense Initative Organization, Innovative Science and Technology Office through an agreement with the National Aeronautics and Space Administration (NASA). Additional support for this work at JPL was provided by the Department of Energy's Catalysis/Biocatalysis Program, Advanced Industrial Concepts Division, through an agreement with NASA. We thank H. Jones for expert technical assistance and J. W. Perry, B. G. Tiemann, D. A. Dougherty, G. R. Meredith, and J. J. Hopfield for helpful discussions.

22 October 1990; accepted 17 January 1991

Reconciling the Magnitude of the Microscopic and Macroscopic Hydrophobic Effects

KIM A. SHARP, ANTHONY NICHOLLS, RICHARD F. FINE, BARRY HONIG*

The magnitude of the hydrophobic effect, as measured from the surface area dependence of the solubilities of hydrocarbons in water, is generally thought to be about 25 calories per mole per square angstrom (cal mol^{-1} Å^{-2}). However, the surface tension at a hydrocarbon-water interface, which is a "macroscopic" measure of the hydrophobic effect, is ≈72 cal mol^{-1} Å^{-2}. In an attempt to reconcile these values, alkane solubility data have been reevaluated to account for solute-solvent size differences, leading to a revised "microscopic" hydrophobic effect of 47 cal mol^{-1} Å^{-2}. This value, when used in a simple geometric model for the curvature dependence of the hydrophobic effect, predicts a macroscopic alkane-water surface tension that is close to the macroscopic value.

HYDROPHOBICITY IS GENERALLY associated with the increases in free energy and heat capacity that are observed when nonpolar solutes are transferred from nonpolar solvents to water (*1, 2*). The observation that the free energy increase is primarily entropic in origin at lower temperatures but becomes increasingly enthalpic as the temperature is raised recently has led to questions about the precise origin of the effect (*3–5*). In this report we focus on the magnitude of the hydrophobic effect in the physiological temperature range. At these temperatures, the free energy change is primarily due to a decrease in entropy that arises from a poorly defined ordering of water molecules around the solute.

Hydrophobic free energies have been obtained from measurements of the solubility of hydrocarbons in water and from partition coefficients of various solutes between aqueous and nonpolar phases. The observed free energy changes have been correlated with accessible surface areas (*6*), and coefficients ranging from 16 to 31 cal mol^{-1} Å^{-2} have been reported (*7–10*). This variation is in part due to the use of different solvents, different measures of surface area, and different approaches to fitting the data.

In this report we focus primarily on aliphatic hydrocarbons because there is a great deal of experimental data available and because these molecules have negligible electrostatic and hydrogen-bonding contributions to solvation. The change in standard state chemical potential, $\Delta\mu^0$, on transfer of

K. A. Sharp, A. Nicholls, B. Honig, Department of Biochemistry and Molecular Biophysics, Columbia University, 630 West 168 Street, New York, NY 10032.
R. F. Fine, Biosym Technologies, Inc., San Diego, CA 92121.

*To whom correspondence should be addressed.

a hydrocarbon from pure liquid to a state of infinite dilution in water (*11*) is usually obtained from the ideal solution expression

$$\Delta\mu^0 = -RT\ln K_X \qquad (1)$$

where R is the gas constant, T is the absolute temperature, and K_X is the partition coefficient between the two phases expressed in mole fractions. From Eq. 1, the addition of a CH_2 group to an alkane increases $\Delta\mu^0$ by ≈880 cal (*1, 12*), whereas increase in accessible area is ≈29 Å^2, giving 30 cal mol^{-1} Å^{-2} for the hydrophobic free energy per unit area (*8*).

A "macroscopic" measure of the hydrophobic free energy per unit area comes from liquid hydrocarbon–water surface tensions, which range from 72 cal mol^{-1} Å^{-2} for pentane to 75 cal mol^{-1} Å^{-2} for decane (*13*). Tanford pointed out the discrepancy between the microscopic and macroscopic values more than 10 years ago (*14*). Because of the widespread use of free energy–surface area relations, it is clearly necessary to reconcile the large difference between the two measures of hydrophobic free energies. We start by reconsidering how values of free energy are extracted from solubility measurements.

When a solute is partitioned between two solvents, equilibrium is achieved when the chemical potential is the same in both phases. The free energy of adding a solute molecule to a solvent consists of contributions from the entropy of mixing, which depends on the concentration of the components, and what might be termed the intrinsic solute-solvent free energy, μ^0, which depends on the strength of the solvent-solute interaction. When solute and solvent are the same size, the entropy of mixing is given by the logarithm of the mole fraction ratio, and Eq. 1 is valid. However, when solute and solvent have different sizes, this expression for the entropy of mixing is no longer valid.

Theories of mixing for solutions of flexible (*15, 16*) and rigid (*17, 18*) solutes that account for solute-solvent size differences provide a more general equivalent to Eq. 1:

$$\Delta\mu^0 \approx -RT\ln K_V - RT\,(V_r^w - V_r^{np}) \qquad (2)$$

K_V is the partition coefficient expressed in volume fraction units, and V_r^w and V_r^{np} are the ratios of the molar volume of solute to the molar volume of solvent in the aqueous and nonpolar phases, respectively. DeYoung and Dill (*19*) successfully used Eq. 2 to account for molecular size differences in the partitioning of benzene between alkanes and water.

We used Eq. 2 to extract transfer energies from the solubilities of *n*-alkanes in water (*12*) and from the partitioning of analogs to aliphatic amino acid side chains between cyclohexane and water (*20*). The liquid-to-water transfer energies for various *n*-alkanes are plotted as a function of accessible surface area in Fig. 1A. Transfer energies obtained from mole fractions (Eq. 1) and volume fractions corrected for differences in molar volume (Eq. 2) are plotted. The slope of the mole fraction curve is 31 cal mol^{-1} Å^{-2}, in agreement with previous analyses. The slope of the corrected volume fraction curve is 47 cal mol^{-1} Å^{-2}, which is near the value reported by DeYoung and Dill for alkanes (*19*). The cyclohexane-water transfer energies of methane, propane, *n*-butane, and isobutane (the side chains of Ala, Val, Leu, and Ile, respectively; *n*-butane and isobutane have identical transfer energies) are also plotted (Fig. 1A). The corrected points fall near the *n*-alkane solubility line.

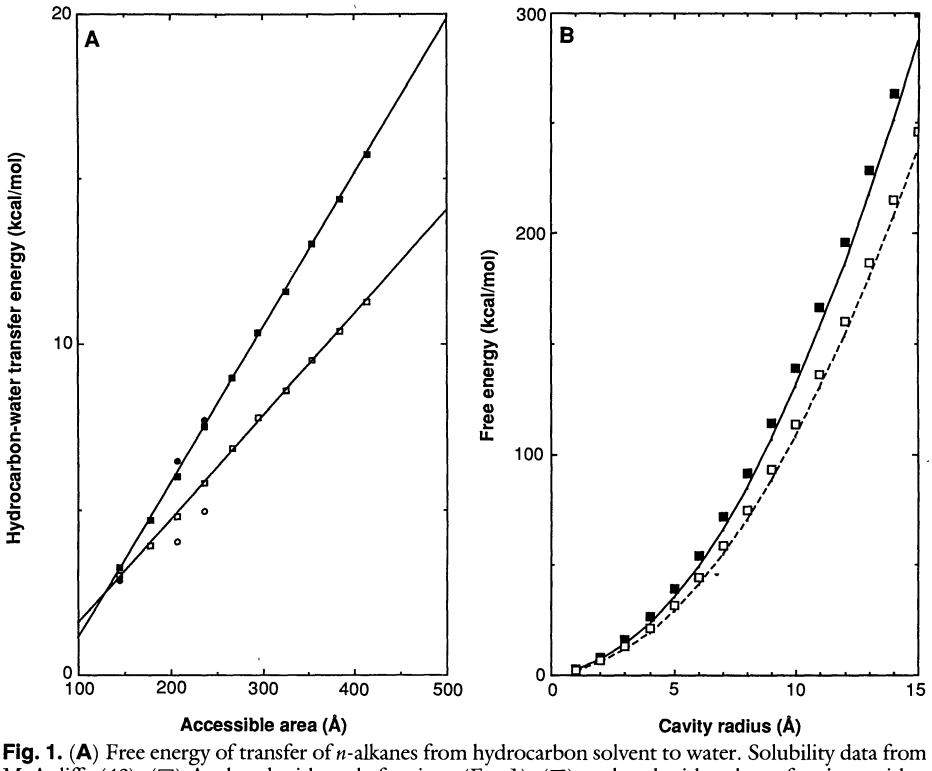

Fig. 1. (**A**) Free energy of transfer of *n*-alkanes from hydrocarbon solvent to water. Solubility data from McAuliffe (*12*). (□) Analyzed with mole fractions (Eq. 1), (■) analyzed with volume fractions with a molar volume correction (Eq. 2), (○) uncorrected cyclohexane-to-water transfer energies (*20*), and (●) corrected cyclohexane-to-water transfer energies. Lines indicate best fits to the solubility data. (**B**) Free energy of cavity formation in water. (———) Scaled particle theory using the parameters from Berendsen and co-workers (*24*), derived from a water model with a density of 0.983 g ml^{-1} and a hard sphere diameter of 2.875 Å and which has a planar surface tension limit of 96.6 cal mol^{-1} Å^{-2}. (- - -) Scaled particle theory using the parameters from Pierotti (*23*) (density, 0.997 g ml^{-1}; hard sphere diameter, 2.75 Å; planar surface tension limit, 79.6 cal mol^{-1} Å^{-2}). (■ and □) Calculated from Eq. 5, assuming a macroscopic vacuum-water surface tension of 96.6 or 79.6 cal mol^{-1} Å^{-2}, respectively.

The results summarized in Fig. 1A account for part of the discrepancy between the hydrophobic effect as measured from microscopic molecular solubilities and from macroscopic surface tension. We demonstrate below that a model that incorporates the radius of curvature of the solute provides a smooth transition between the microscopic and macroscopic regimes.

The idea that the surface free energy has a curvature dependence dates back to a thermodynamic theory due to Tolman (*21*):

$$\gamma(r)/\gamma(\infty) = 1/(1 + 2\delta/r) \qquad (3)$$

where $\gamma(r)$ is the surface tension of a convex surface of radius r and δ is an unknown constant of atomic dimensions. Eyring and co-workers (*22*) used this expression to correlate the size and solubility of gases in nonpolar liquids. We have found that a similar expression can be derived from simple geometric considerations.

The free energy increase that occurs when a water molecule is located near an interface with a nonpolar surface is due to the exclusion of other water molecules from the nonpolar region. We introduce the simple assumption that the change in free energy is proportional to the resultant loss in accessible surface area of this water. This, in turn, is proportional to the solid angle excluded by the interface, as shown in Fig. 2A. For a spherical interface, the excluded solid angle is $\theta = 2\pi(1 + a/R)$, where a is the radius of a water molecule and R is the radius of curvature of the interface. With interfacial

free energy proportional to excluded area, the following expression can be obtained:

$$\gamma(R)/\gamma(\infty) = 1/(1 \pm a/R) \quad (4)$$

The negative sign in Eq. 4 is for concave surfaces. For convex surfaces, it is striking that a simple geometric model leads to an expression identical to Tolman's when 2δ of Eq. 3 is set equal to the radius of a water molecule.

We compared the predictions of Eq. 4 with those of scaled particle theory, which relates the free energy of forming a spherical cavity in a particular solvent to the cavity radius, the hard-sphere diameter, and the density of the solvent. Pierotti (*23*) has applied the theory to the formation of a cavity in water using the experimental O–O distance for the hard-sphere diameter and the known density of water. The macroscopic surface tension (that is, at infinite solute radius) is then 79.6 cal mol^{-1} $Å^{-2}$, somewhat less than the air-water surface tension of 102 cal mol^{-1} $Å^{-2}$. Berendsen and coworkers (*24*) instead used the parameters of the scaled point charge water model (*25*) and obtained a macroscopic limit of 96.6 cal mol^{-1} $Å^{-2}$.

We plot the predictions of scaled particle theory as a function of cavity radius, using the parameters of Pierotti and of Berendsen and co-workers and the values obtained from Eq. 4, where $\gamma(\infty)$ = 96.6 or 79.6 cal mol^{-1} $Å^{-2}$ (Fig. 1B). Independent of the parameters used in scaled particle theory, the geometric model of Eq. 4 accurately reproduces the predicted curvature dependence. Simulations of the free energy of cavity formation (*24, 26*) are also in excellent agreement with the predictions of scaled particle theory and thus with Eq. 4. Remarkably, each of these quite different models produces similar curvature dependences for the surface tension.

In the derivation of Eq. 4, it was assumed that the water-water interaction is independent of radius of curvature, which ignores possible energetic consequences of changes in the structure of water as the curvature changes. Computer simulations show that water around small spherical cavities maintains all possible hydrogen bonds (at an entropic cost) (*24*), whereas water near planar surfaces sacrifices a hydrogen bond (*27*). These results might suggest that a model based on curvature alone would be unable to bridge the microscopic and macroscopic regimes. However, the formation of a macroscopic interface is associated with an increase in both enthalpy and entropy (*28, 29*), indicating that increased motion of surface water compensates for the loss of hydrogen bonds. This would indicate that the phenomenon of enthalpy-entropy compensation allows for the possibility of a smooth transition between the microscopic and macroscopic hydrophobicity.

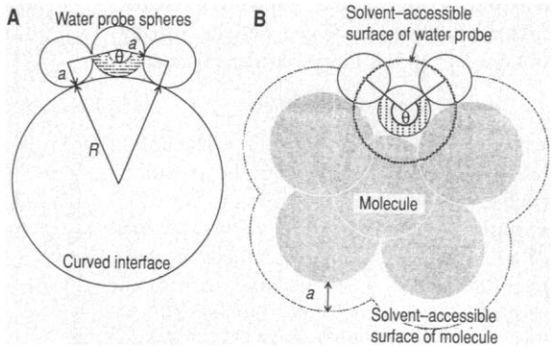

Fig. 2. Water at curved interfaces. The degree of inaccessibility of the central water probe sphere to other water molecules at a curved interface is indicated by its shaded area, subtending a solid angle of θ steradians. (**A**) For a plane $\theta = 2\pi$, for a spherical interface of curvature R, by construction $\theta = 2\pi/(1 + a/R)$. (**B**) For an irregular molecular interface, $\theta/4\pi$ is the fraction of the water's solvent-accessible surface lying within the molecule's solvent-accessible surface.

Equation 4 is only applicable for spherical interfaces and clearly breaks down for complex geometries. However, real molecules can be treated while still retaining the assumption that hydrophobicity is related to the area of a water molecule that is excluded by the interface. We have developed an algorithm (*30*) in which a water molecule is placed at a series of points on the accessible surface of an interface. The solid angle, θ, excluded by the interface at each point is obtained from the fraction of the accessible area of the water molecule that lies within the accessible area of the molecule of interest (Fig. 2B). The curvature-corrected surface free energy at that point is given by $\gamma(x) = C\gamma(\infty)$, where $C = \theta/2\pi$. One can obtain mean curvatures for atoms or subgroups of the molecule by averaging C over all accessible surface points corresponding to that group.

For a CH_2 group in an alkane chain, C is 0.8. If one uses a value of 47 cal mol^{-1} $Å^{-2}$, which is the slope of the corrected free energy versus surface area curve for alkanes, Eq. 4 predicts a value for $\gamma(\infty)$ of 59 cal mol^{-1} $Å^{-2}$. This value approaches, but is still somewhat below, the macroscopic value of 72 to 75 cal mol^{-1} $Å^{-2}$.

To make a precise comparison between microscopic and macroscopic surface tension, one must account for two additional factors: the molecular roughness of the alkane surface and the disorder or fluctuations of the interface. One may estimate the effect of molecular roughness by treating the hydrocarbon side of the interface as close-packed spheres of radius 2 Å (a reasonable radius for a methyl group), which gives a macroscopic planar area ≈20% smaller than the surface area accessible to water (used in evaluating the solubility data). The effect of random thermal fluctuations of the interface can be estimated with the aid of a theory attributable to Buff and co-workers that describes these fluctuations as a superposition of thermally driven capillary wave modes (*31*). For liquid alkane–water systems, this theory predicts a root-mean-square fluctuation of ≈4.5 Å, which contributes about 4.1 cal mol^{-1} $Å^{-2}$ to the surface tension (*30*). Applying the effects of roughness and fluctuations to the value of $\gamma(\infty)$ derived from the corrected solubility data, one obtains a surface free energy of ≈67 calorie per mole per square angstrom of macroscopic area.

Because of the approximations inherent in our treatment, the agreement is satisfactory between the two surface free energy values, one determined from solubility measurements and one from surface tension. This suggests that the discrepancy between the microscopic and macroscopic hydrophobic effects may have been resolved. Moreover, the use of simple geometric arguments makes it possible to obtain a simple definition for local, curvature-dependent hydrophobicities that vary over the accessible surface. Our results imply that all "hydrophobicity scales" that have been derived from solubility data with the use of Eq. 1 significantly underestimate the magnitude of the hydrophobic effect. It appears that large interfaces, particularly in concave regions such as protein binding sites, can be far more hydrophobic than previously suspected. Finally, the significant error incurred when mole fractions are used to evaluate solubility data suggests that the agreement reported between the results of theoretical simulations and experimental solvation energies may have to be reevaluated.

REFERENCES AND NOTES

1. C. H. Tanford, *The Hydrophobic Effect* (Wiley, New York, 1980).
2. R. Baldwin, *Proc. Natl. Acad. Sci. U.S.A.* **83**, 8069 (1986).
3. P. L. Privalov and S. J. Gill, *Adv. Protein Chem.* **39**, 191 (1988).
4. K. P. Murphy, P. L. Privalov, S. J. Gill, *Science* **247**, 559 (1990).
5. K. A. Dill, *ibid.* **250**, 297 (1990).
6. The accessible surface area is defined as the locus of points available to the center of a water molecule "rolling" around the solute; see B. Lee and F. M. Richards [*J. Mol. Biol.* **55**, 379 (1971)]. It is standard to use the area of the extended alkane chain; see (8, 9).
7. C. Chothia, *J. Mol. Biol.* **105**, 1 (1976).
8. R. B. Hermann, *Proc. Natl. Acad. Sci. U.S.A.* **74**, 4144 (1977).

9. J. A. Reynolds, D. B. Gilbert, C. Tanford, *ibid.* **71**, 2925 (1974).
10. D. Eisenberg and A. D. McLachlan, *Nature* **319**, 199 (1986).
11. A. Ben-Naim, *J. Phys. Chem.* **82**, 792 (1978).
12. C. McAuliffe, *ibid.* **70**, 1267 (1966).
13. R. Aveyard and D. A. Haydon, *J. Colloid Interface Sci.* **20**, 2255 (1965).
14. C. H. Tanford, *Proc. Natl. Acad. Sci. U.S.A.* **76**, 4175 (1979).
15. P. J. Flory, *J. Chem. Phys.* **9**, 660 (1941).
16. M. L. Huggins, *ibid.*, p. 440.
17. J. H. Hildebrand, *ibid.* **15**, 225(1947).
18. G. A. Mansoori, N. F. Carnahan, K. E. Starling, T. W. Leland, *ibid.* **54**, 1523 (1971).
19. L. R. DeYoung and K. A. Dill, *J. Phys. Chem.* **94**, 801 (1990).
20. A. Radzicka and R. Wolfenden, *Biochemistry* **27**, 1664 (1988).
21. R. C. Tolman, *J. Chem. Phys.* **17**, 333 (1949).
22. D. S. Choi, M. S. Jhon, H. Eyring, *ibid.* **53**, 2608 (1970).
23. R. A. Pierotti, *J. Phys. Chem.* **69**, 281 (1965).
24. J. P. Postma, H. J. Berendsen, J. R. Haak, *Faraday Symp. Chem. Soc.* **17**, 55 (1982).
25. H. J. Berendsen, J. R. Grigera, T. P. Straatsma, *J. Phys. Chem.* **91**, 6269 (1987).
26. R. Fine and X. Ni, unpublished results.
27. C. Y. Lee, J. A. McCammon, P. J. Rossky, *J. Chem. Phys.* **80**, 4448 (1984).
28. W. D. Harkins and Y. C. Cheng, *J. Am. Chem. Soc.* **43**, 35 (1921).
29. A. W. Adamson, *Physical Chemistry of Surfaces* (Wiley, New York, 1976).
30. A. Nicholls, K. Sharp, R. Friedman, B. Honig, unpublished results.
31. F. P. Buff, R. A. Lovett, F. H. Stillinger, *Phys. Rev. Lett.* **15**, 621 (1965).
32. We thank K. Dill and R. Friedman for helpful discussions and P. Rossky for his careful reading of the manuscript. Supported by the NIH (grants GM30518 and GM41371) and NSF (grant DMB 88-05434).

8 November 1990; accepted 31 January 1991

A New Mechanism for the Formation of Meteoritic Kerogen-Like Material

WINDSOR A. MORGAN, JR.,* ERIC D. FEIGELSON, HAI WANG, MICHAEL FRENKLACH

The carbon in ancient carbonaceous chondritic meteorites is mainly in a hydrocarbon composite similar to terrestrial kerogen, a cross-linked structure of aliphatic and aromatic hydrocarbons. Until recently, the composite has been commonly thought to have been produced in the early solar nebula by a Fischer-Tropsch–type process, involving the catalytic synthesis of hydrocarbons from carbon monoxide and hydrogen on grain surfaces. Instead, the aromatic hydrocarbons may form in gas-phase pyrolysis of simple aliphatics like acetylene and methane by a mechanism developed recently to explain formation of soot in combustion and of aromatic molecules in circumstellar envelopes. Nonequilibrium chemical kinetic calculations indicate that this mechanism can produce meteoritic aromatics if the initial concentration of simple hydrocarbons in the solar nebula was sufficiently but not unreasonably high.

THE COMPLEX NATURE OF C-BEARING material in carbonaceous chondritic meteorites has been a subject of great interest for several decades. Components such as racemic mixtures of prebiological amino acids and tiny refractory particles of presolar diamond constitute only a small amount of the C in these meteorites (*1*). Most C resides in the matrix as a hydrocarbon composite similar to the terrestrial material "kerogen," which is an acid-insoluble material comprised of aliphatic and aromatic hydrocarbons found in coal and humic soil (*2*). The meteoritic material is variously referred to as "kerogen-like material," "insoluble carbon," or "macromolecular carbon." The aromatic fraction can reach 75% and is comprised mainly of 1- to 8-ring molecules (*3*).

Attempts to explain the origin of meteoritic kerogen-like material generally assumed (as we do) that it formed in the early solar nebula, although recent evidence for polycyclic aromatic hydrocarbon (PAH) molecules in the interstellar medium (*4*) permits that some material could have been inherited from the parent interstellar cloud. The two formation mechanisms generally considered have been: (i) photolysis of various combinations of CH_4, C_2H_6, NH_3, H_2S, and H_2O by energetic radiation, as in Miller-Urey experiments (*5*); and (ii) the reaction of CO and H_2 on the surface of mineral catalysts through Fischer-Tropsch–type (FTT) reactions (*6*).

The FTT synthesis has attracted the most attention (7), but it has several drawbacks. Foremost among them, and directly motivating our work, is that the FTT process under terrestrial conditions typically produces almost exclusively aliphatic hydrocarbons (*8*). In experiments simulating solar nebula conditions, Studier *et al.* (*9*) reported up to a 35% yield of aromatics, but only after reheating to about 1200 K when aliphatic hydrocarbon species were already present. These aliphatics, rather than CO, are more likely to be the precursors of the aromatic product under their experimental conditions. Also, the reported prevalence of certain meteoritic aliphatic species, which closely matched FTT predictions (*9*), probably resulted from terrestrial contamination (*10*). Because the most widely discussed explanation for the formation of this material has encountered such difficulties, there is considerable motivation to investigate alternatives.

We propose that aromatic hydrocarbon formation takes place in the gas phase by pyrolysis of simple hydrocarbons present in the solar nebula, such as acetylene (C_2H_2) or methane (CH_4). Our model is based on the detailed chemical kinetic mechanism developed recently by Frenklach and colleagues to explain the early stages of soot formation in hydrocarbon pyrolysis and combustion (*11*). The first aromatic ring can be formed through one of several possible pathways. The principal growth pathway of the mechanism is the abstraction of H atoms, followed by the addition of C_2H_2 molecules to the resulting aromatic radical. Essentially the same mechanism has been applied to investigate PAH formation in the dense atmospheres of carbon-rich red-giant stars (*12, 13*). At high temperatures ($T \sim$ 2000 K), where PAH molecules form in terrestrial flames, aromatic formation does not occur in stars because ambient H_2 inhibits the abstraction step. However, at lower temperatures (900 K $\leq T \leq$ 1100 K) the H-abstraction is no longer the rate-limiting step, and the reaction is driven by the irreversibility of the C_2H_2 addition. For sufficiently dense and slow winds, the aromatic yield in C stars can approach 100% of the initial C in C_2H_2 (*12*).

The chemical reaction mechanism is composed of two parts. The first (*14*) is responsible for the interconversion between CH_4 and C_2H_2 and determines the concentration of H atoms, the main reaction carrier under the conditions studied. The second reaction subset (*12*) describes the formation and growth of PAH molecules starting from C_2H_2. Altogether the model contains more than 200 reactions and computes the time-

W. A. Morgan, Jr., and E. D. Feigelson, Department of Astronomy and Astrophysics, The Pennsylvania State University, 525 Davey Laboratory, University Park, PA 16802.
H. Wang and M. Frenklach, Department of Materials Science and Engineering, The Pennsylvania State University, 202 Academic Projects Building, University Park, PA 16802.

*To whom correspondence should be addressed.